CHAPTER 2

B-SPLINE BASED EMPIRICAL MODE DECOMPOSITION

Sherman Riemenschneider, Bao Liu, Yuesheng Xu and Norden E. Huang

This paper discusses some mathematical issues related to empirical mode decomposition (EMD). A B-spline EMD algorithm is introduced and developed for the convenience of mathematical studies. The numerical analysis using both simulated and practical signals and application examples from vibration analysis indicate that the B-spline algorithm has a comparable performance to that of the original EMD algorithm. It is also demonstrated that for white noise, the B-spline algorithm acts as a dyadic filter bank. Our mathematical results on EMD include Euler splines as intrinsic mode functions, the Hilbert transform of B-splines, and the necessary and sufficient conditions which ensure the validity of the Bedrosian identity of the Hilbert transform of product functions.

2.1. Introduction

Information processing is important in both pure research and practical applications. More often than not, information is embedded in data corrupted by noise. With the rapid development of science and technology, we are now inundated with a voluminous amount of data every day. The data need to be processed to extract meaningful information for various applications. Fourier transform is the most used and powerful traditional technique of data analysis. However, this technique is not effective in processing non-stationary and nonlinear signals because the basis functions it uses are not localized and cannot properly characterize the spectrum evolution in time. Time-frequency analysis is considered the major approach for overcoming the limitations of the traditional techniques. It aims at representing a signal with a joint function of both time and frequency, thereby providing a revealing picture in the time-frequency domain that allows the investigation of the non-stationary and nonlinear characteristics of a signal.

For over fifty years, researchers have put significant effort into seeking effective and efficient ways of time-frequency representation. Short-time Fourier transform (Gabor 1946; Cohen 1995; Qian 1996), a representative achievement of this effort, is powerful in various applications. Unfortunately, it has difficulties in processing some types of signals such as those composed of small bursts plus quasi-stationary components because its time and frequency resolution is fixed. Although a number of improved methods have been developed by adapting the window size to the

local composition of a signal (cf., Jones and Park 1990), these methods are either computationally expensive or effective only for certain specific applications. The Wigner-Ville distribution (Cohen 1995; Qian 1996) is another classical technique. It can well preserve the time and frequency concentration of a signal but has the drawback of cross-term interference, which often obscures the useful pattern over the time-frequency plane. To overcome this problem, various techniques (Choi and Williams 1989; Zhao et al. 1990), have been developed based on Cohen's general framework, (Cohen 1966) with the aim of reducing the cross-term interference while retaining the desirable properties of Wigner-Ville distribution. The recent advances of wavelet analysis opened a new path for time-frequency analysis. A significant breakthrough of wavelet analysis was the use of multi-scales to characterize signal events. This technique has led to the development of several wavelet-based time-frequency analysis techniques (Daubechies 1992; Mallat 1998). Some of them are adaptive, such as wavelet packets (Coifman et al. 1992), matching pursuit (Mallat and Zhang 1993), and basis pursuit (Chen et al. 2001). Despite the great success of numerous applications, all the above-mentioned techniques, however, each have their own limitations, and almost all of them are ineffective for characterizing the detailed time-frequency composition of nonlinear signals. On the other hand, most of the existing nonlinear time series analysis methods (Diks 1999) are designed only for stationary systems.

Over the past several decades, researchers have been attempting to exploit the concept of instantaneous frequency derived from analytic signals to construct a time-frequency representation. It is expected that such a representation may not have the fundamental drawbacks in the above-mentioned techniques. However, due to the existence of some paradoxes involving the instantaneous frequency derived this way and the concept of frequency in Fourier analysis or in our intuition (Cohen 1995), this effort did not have much success until Huang et al. (1998, 1999) developed the empirical mode decomposition (EMD) method. This method is now known as Hilbert–Huang transform (HHT) in the literature. It provides a powerful tool for improving the time-frequency technology. The basic approach of the EMD method is to decompose a signal into a collection of intrinsic mode functions (IMF) that allow well-behaved Hilbert transforms for computation of physically meaningful instantaneous frequencies. This consequently makes it possible to construct a time-frequency representation, known as the "Hilbert spectrum," by using instantaneous frequency. Another breakthrough is that, unlike wavelet analysis, which characterizes the scale of a signal event with pre-specified basis functions, HHT decomposes a signal by direct extraction of the local energy associated with the intrinsic time scales of the signal itself. The Hilbert spectrum, therefore, can depict not only the inter- but also the intra-wave time-frequency characteristics of a local event. Thus, HHT is applicable to both non-stationary and nonlinear signals.

HHT has been proved remarkably effective in various applications (Echeverria et al. 2001; Pines and Salvino 2002; Zhang et al. 2003). However, most of the underlying

mathematical problems has still not been treated. As HHT finds wider and wider applications, the need for a rigorous mathematical foundation becomes more urgent. Recently, in the attempt to circumvent the mathematical difficulties, Chen et al. (2004) developed a variation of the original EMD, which appears potentially more convenient for an analytical formulation of EMD and for the study of certain related mathematical issues. This method represents the local mean of a signal by using the moving averages of the extrema as combinations of B-splines and avoids the use of envelopes, for which a proper mathematical definition is still an unsolved issue. In addition, this method overcomes the problem that, in implementation of the original EMD, the upper and lower envelopes may cross. Recently, we applied this method in an analysis of vibration signals for equipment fault diagnosis (Liu et al. 2004). The results showed that this method had a comparable performance to that of the original EMD.

The present paper reviews the work on the B-spline EMD (BS-EMD) based on Chen et al. (2004), Liu et al. (2004), and Xu and Yan (2004). In the next section, the algorithm of BS-EMD is reviewed. Then in section 2.3, some related mathematical results are presented, including Euler splines as a prototypical examples of B-spline IMFs, the properties of the Hilbert transform of B-splines, and the necessary and sufficient conditions which ensure the validity of the Bedrosian identity of the Hilbert transform of product functions. Section 2.4 addresses the properties of the BS-EMD as a filter bank and investigates the performance of the BS-EMD through comparison with the original EMD. In section 2.5, we present some application examples of the BS-EMD method and its corresponding Hilbert spectrum in vibration signal analysis. Finally, in section 2.6, the conclusion is presented and future research problems are outlined.

2.2. A B-spline algorithm for empirical mode decomposition

The empirical mode decomposition method decomposes a signal into a finite sum of intrinsic mode functions that allow the computation of a physically meaningful instantaneous frequency defined in terms of the Hilbert transform. To describe the B-spline algorithm for empirical mode decomposition, we first recall the definition of the Hilbert transform. For a real signal $s(t)$, the Hilbert transform is defined by the principal value (PV) integral

$$\mathcal{H}s(t) := \frac{1}{\pi}\mathrm{PV}\int_{-\infty}^{\infty}\frac{s(\tau)}{t-\tau}\,d\tau\,. \tag{2.1}$$

This yields an analytic signal

$$Z(t) = s(t) + i\mathcal{H}s(t) = a(t)e^{i\theta(t)}\,, \tag{2.2}$$

with

$$a(t) = \sqrt{s(t)^2 + \mathcal{H}s(t)^2}, \qquad \theta(t) = \arctan\left[\frac{\mathcal{H}s(t)}{s(t)}\right]\,, \tag{2.3}$$

where $a(t)$ and $\theta(t)$ are the amplitude and phase, respectively, of the signal at time t. The instantaneous frequency can be computed by

$$\omega(t) = \frac{d\theta(t)}{dt}. \tag{2.4}$$

Note that both the amplitude and instantaneous frequency in the above are functions of time. We naturally hope to construct a time-frequency representation by using the Hilbert transform. If this representation were correct for any arbitrary signal, we would have a time-frequency representation with a higher energy concentration than that of the short-time Fourier transform and wavelet transform, and a clearer representation pattern than that of the Wigner-Ville distribution. Unfortunately, a significant difficulty is that the instantaneous frequency obtained in this way may have frequency values which are meaningless in physics. This problem has plagued researchers for many years because the attempts to overcome it have been based on classical Fourier methods and filter theory.

The development of the EMD is a method for solving the above-mentioned problem. Huang et al. (1998) found that to define a meaningful instantaneous frequency for a function by using the Hilbert transform, the function has to satisfy the following two conditions:

(1) The number of the extrema and the number of the zero crossings of the function must be equal or differ at most by one.
(2) At any point of the function, the mean value of the envelopes defined by the local extrema should be zero.

Such a function is called the "intrinsic mode function" (IMF). Since the IMFs defined in this way admit computation of meaningful instantaneous frequencies, it becomes possible to construct a time-frequency representation based on the Hilbert transform.

The EMD algorithm provides a method to obtain the IMFs with the basic idea being the removal of the local mean from a signal by using a sifting process. In the original EMD, the local mean is computed as the mean value of the upper and lower envelopes. The envelopes themselves are approximated as the cubic spline interpolant of the local maxima and local minima, respectively. It can be seen that "envelopes" play a crucial role in this algorithm. However, a good mathematical description of envelopes remains an unsolved issue. For the convenience of studying the mathematical foundation of the EMD method, a more direct link from the local extrema to the mean in the sifting process is desirable. This need led to the development of the B-spline algorithm of EMD (Chen et al. 2004). It uses the moving average of the extrema as combinations of B-splines and is very amenable to mathematical study. We present the basic idea of the BS-EMD from Chen et al. (2004) in the following.

We first define the B-splines of order k for an arbitrary knot sequence (De Boor 1978). For a given increasing sequence τ_j, $j \in Z$, the jth B-spline of order k is defined

by the kth order divided difference, $[\tau_j, \ldots, \tau_{j+k}]$, at the $k+1$ points $\tau_j, \ldots, \tau_{j+k}$ applied to the truncated power as a function of x

$$B_{j,k,\tau}(t) := (\tau_{j+k} - \tau_j)\,[\tau_j, \ldots, \tau_{j+k}]\,(x-t)_+^{k-1}, \qquad t \in \mathbb{R}, \tag{2.5}$$

where $(x-t)_+^{k-1}$ is zero if $x < t$ and equals $(x-t)^{k-1}$ if $x \geq t$. These B-splines form a basis for the space of splines of order k with knots τ_j, $j \in Z$. In other words, for any function s in this space, there exist unique scalars a_j such that

$$s(t) = \sum_{j \in Z} a_j B_{j,k,\tau}(t), \qquad t \in \mathbb{R}. \tag{2.6}$$

B-splines satisfy the following recursive formula

$$B_{j,k,\tau}(t) = \frac{t - \tau_j}{\tau_{j+k-1} - \tau_j} B_{j,k-1,\tau}(t) + \frac{\tau_{j+k} - t}{\tau_{j+k} - \tau_{j+1}} B_{j+1,k-1,\tau}(t), \tag{2.7}$$

with

$$B_{j,1,\tau}(t) = \begin{cases} 1, & \tau_j \leq t < \tau_{j+1}, \\ 0, & \text{elsewhere.} \end{cases} \tag{2.8}$$

They are normalized so that

$$\sum_{j=p}^{q} B_{j,k,\tau}(t) = 1, \qquad q \geq p + k, \tag{2.9}$$

on $[\tau_{p+k-1}, \tau_{q+1}]$.

For use in EMD, we define an operator on a given signal s as follows: The knots $\tau^s := \{\tau_j : j \in Z\}$ are taken as the extreme points of s. The knots in the support of the B-spline B_{j,k,τ^s} of order k are τ_{j+l}, $l = 0, 1, \ldots, k$ with B_{j,k,τ^s} vanishing outside (τ_j, τ_{j+k}) and strictly positive inside that interval (hence, at $\tau_{j+1}, \ldots, \tau_{j+k-1}$). At these extreme points strictly inside the support of B_{j,k,τ^s}, the following linear functionals are defined:

$$\lambda_{j,k,\tau^s} : s \mapsto \frac{1}{2^{k-2}} \sum_{l=1}^{k-1} \binom{k-1}{l} s(\tau_{j+l}). \tag{2.10}$$

This definition is a binomial average of the extrema contained in the support of B_{j,k,τ^s}, where more weight is given toward the center of the support. We take

$$V_{\tau^h,k} s := \sum_{j \in Z} \lambda_{j,k,\tau^s}(s) B_{j,k,\tau^s} \tag{2.11}$$

as the operator to replace the mean envelope in the original EMD algorithm.

As particular examples, when $k = 3$, we have the quadratic B-spline approximation

$$V_{\tau^s,3} s := \sum_{j \in Z} \tfrac{1}{2} [s(\tau_{j+1}) + s(\tau_{j+2})]\, B_{j,3,\tau^s}, \tag{2.12}$$

and when $k = 4$, we have the cubic B-spline approximation

$$V_{\tau^s,4}s := \sum_{j\in Z} \tfrac{1}{4}\left[s(\tau_{j+1}) + 2s(\tau_{j+2}) + s(\tau_{j+3})\right] B_{j,4,\tau^s}\,. \tag{2.13}$$

Using the operator defined above, we obtain the B-spline algorithm for the empirical mode decomposition. This algorithm extracts the first IMF of a signal s by using the following sifting process:

(1) Find the local extrema of s.
(2) Apply the operator $V_{\tau^h,k}$ in (2.11) to s.
(3) Compute $h = s - V_{\tau^h,k}s$.
(4) If h is an IMF, stop. Otherwise, treat h as the signal and iterate on h through Steps 1 to 4.

Denote by c_1 the first IMF and set $r_1 = s - c_1$, the first residue. The algorithm proceeds to select the next IMF by applying the above procedure to the first residue r_1. This process is repeated until the last residue r_n has at most one extremum (excluding the ends) or becomes constant. The original signal then can be represented as

$$s = \sum_{j=1}^{n} c_j + r_n\,. \tag{2.14}$$

As in Huang et al. (1998), the stopping condition in Step 4 is to limit the following standard deviation from two consecutive results in the sifting process:

$$SD = \sum_{t=0}^{T} \frac{[h_{m-1}(t) - h_m(t)]^2}{h_{m-1}^2(t)}\,, \tag{2.15}$$

where T is the length of the signal, and h_m, the sifting result in the mth iteration. A typical stopping value of SD is set between 0.2 and 0.3.

Our numerical studies show that after a finite number of iterations, the sifting result of the BS-EMD will be an IMF. After applying the Hilbert transform on each IMF, we obtain an analytic signal corresponding to the signal $s(t)$

$$z(t) = \sum_{j=1}^{n} a_j(t) \exp\left[i \int_{-\infty}^{t} \omega_j(\tau)\, d\tau\right] + r_n(t)\,. \tag{2.16}$$

The first term on the right side of (2.16) can be considered as a generalization of the Fourier expansion. It differs from the latter in that the components in (2.16) have a variable amplitude and frequency. This allows the amplitude and the frequency modulation to be separated and makes possible the conversion of the signal to a joint function of time and frequency. The residue r_n characterizes the trend of the signal and can be treated separately.

2.3. Some related mathematical results

In this section, we review some mathematical results related to IMFs, Hilbert transforms and the Bedrosian identity in the context of EMD. Most of the results discussed in this section come from Chen et al. (2004) and Xu and Yan (2004).

IMFs obtained from the EMD algorithm admit a physically meaningful instantaneous frequency. However, the mathematical definition and characterization of IMFs remain unsolved. We present an illuminating mathematical example of IMFs which is very insightful for further development in the mathematical characterizations of IMFs. An interesting observation is that the Euler splines of Schoenberg are an important class of spline type intrinsic mode functions which tend to the simplest IMF, the harmonic signal, when their degree tends to infinity.

We now recall the definition of Euler polynomials and Euler splines. The Euler polynomial of degree zero is defined by $p_0 = 1$, and Euler polynomials of higher degree are defined recursively by

$$p_n'(t) := np_{n-1}(t), \qquad t \in \mathbb{R}, \qquad n > 1 \tag{2.17}$$

under the constraint conditions $p_n(0) = -p_n(1)$. Specifically, the Euler polynomials of lower order are

$$p_1(t) = t - \tfrac{1}{2}, \quad p_2(t) = t^2 - t, \quad p_3(t) = t^3 - \tfrac{3}{2}t^2 + \tfrac{1}{4}, \tag{2.18}$$

$$p_4(t) = t^4 - 2t^3 + t, \quad p_5(t) = t^5 - \tfrac{5}{2}t^4 + \tfrac{5}{2}t^2 - \tfrac{1}{2}, \quad p_6(t) = t^6 - 3t^5 + 5t^3 - 3t. \tag{2.19}$$

The simplest Euler spline is the piecewise constant periodic function

$$E_0(t) = \operatorname{sgn}[\sin(\pi t)]. \tag{2.20}$$

In general, by using Euler polynomials, Euler splines are generated as follows: Define splines E_n on $\mathbb{R}$ as extensions of the Euler polynomials p_n on $[0, 1]$ to all of $\mathbb{R}$ via the functional equation

$$E_n(t+1) = -E_n(t), \qquad t \in \mathbb{R}. \tag{2.21}$$

That is,

$$E_n(t) := (-1)^{[t]} p_n(t - [t]), \qquad t \in \mathbb{R}. \tag{2.22}$$

Schoenberg's Euler splines $\mathcal{E}_n$ are defined to be

$$\mathcal{E}_n(t) := \begin{cases} E_n(t)/E_n(0), & \text{if } n \text{ is odd;} \\ E_n(t - 1/2)/E_n(1/2), & \text{if } n \text{ is even.} \end{cases} \tag{2.23}$$

Note that Euler splines are 2-periodic piecewise polynomials.

Figure 2.1 shows that Euler splines are non-stationary signals since their frequencies vary with time. However, the instantaneous frequencies of Euler splines

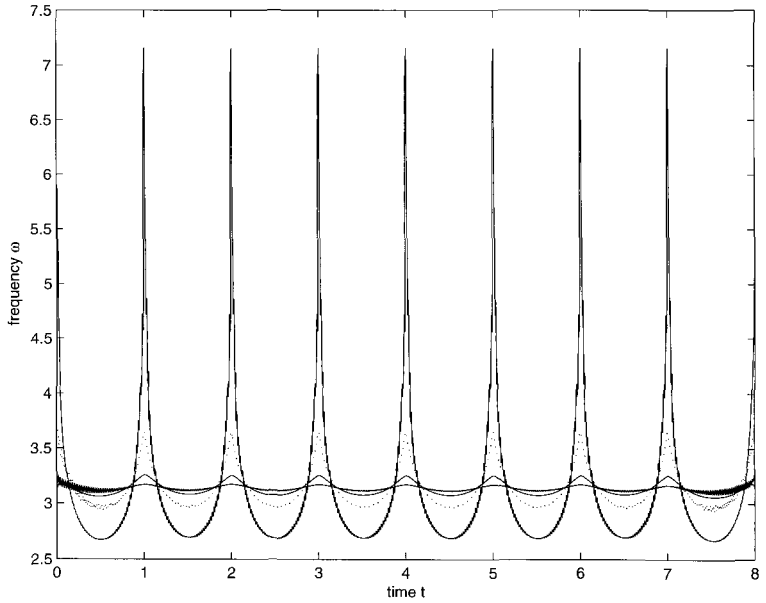

Figure 2.1: The comparisons of instantaneous frequency of Euler splines: The curve with the highest variation is the instantaneous frequency of $\mathcal{E}_2$. The curve of dotted line denotes that of $\mathcal{E}_3$. The remaining two curves of solid lines are the instantaneous frequency of $\mathcal{E}_4$ and $\mathcal{E}_5$. The variation of the instantaneous frequency decreases from $\mathcal{E}_2$ to $\mathcal{E}_5$, and the instantaneous frequency of $\mathcal{E}_5$ is already very close to π.

tend rather rapidly to π when the order of the splines tends to infinity. This observation can be explained by the interesting results of Schoenberg (1964, 1972, 1976, 1983) and Golitschek (1972), which state that,

$$\lim_{n\to\infty} \mathcal{E}_n(t) = \cos(\pi t), \quad \text{uniformly for} \quad t \in \mathbb{R}, \tag{2.24}$$

and

$$\lim_{n\to\infty} \mathcal{E}_{2n-1}^{(k)}(t) = \cos^{(k)}(\pi t), \quad \text{uniformly for} \quad t \in \mathbb{R}, \quad \text{for each} \quad k \in \mathbb{N}. \tag{2.25}$$

In fact, from (6.10) in Schoenberg (1976), the first of these can be quantified as

$$\mathcal{E}_n(t) = \frac{\sum_{\nu=0}^{\infty} \frac{(-1)^{\nu(n+1)}}{(2\nu+1)^{n+1}} \cos[\pi(2\nu+1)t]}{\sum_{\nu=0}^{\infty} \frac{(-1)^{\nu(n+1)}}{(2\nu+1)^{n+1}}} = \cos(\pi t) + O[3^{-(n+1)}]. \tag{2.26}$$

By the absolute convergence of the series in (2.26), it also follows easily that

$$\lim_{n\to\infty} \mathcal{H}\mathcal{E}_n(t) = \sin(\pi t), \text{uniformly for} \quad t \in \mathbb{R}, \tag{2.27}$$

with the same error bound. Thus,

$$\lim_{n\to\infty} \left\{ [\mathcal{E}_n(t)]^2 + [\mathcal{H}\mathcal{E}_n(t)]^2 \right\} = 1, \quad t \in \mathbb{R}. \tag{2.28}$$

B-splines play a crucial role in the BS-EMD algorithm since except for the first IMF, all the others are linear combinations of B-splines. Furthermore, cubic splines used for interpolation of the envelopes in the original EMD can also be written as linear combinations of B-splines. Since time-frequency representation is obtained from the Hilbert transform of each IMF, it is desirable to consider the Hilbert transform of B-splines. Recursive formulas of the Hilbert transform of B-splines were established in Chen et al. (2004). We now review that paper's main results regarding the recursive formulas.

We recall the definition of equally spaced cardinal B-splines. Let χ_I denote the characteristic function of the interval I. We set $B_1 = \chi_{[0,1)}$ and cardinal B-splines of higher orders are defined recursively by convolution with B_1; that is,

$$B_n = B_{n-1} * B_1 = B_1 * B_{n-1}, \quad n = 2, 3, \ldots . \tag{2.29}$$

It can be seen that B_n is a spline of order n with the knots at integers $j = 0, 1, \ldots, n$. Cardinal B-splines enjoy many nice properties (cf., De Boor 1978). If we let $\bigtriangledown$ denote the backward difference operator defined recursively by

$$\bigtriangledown f(\cdot) = f(\cdot) - f(\cdot - 1) \quad \text{and} \quad \bigtriangledown^j = \bigtriangledown \left(\bigtriangledown^{j-1}\right), \tag{2.30}$$

the derivative of the B-splines have the form

$$\frac{d^j}{dt^j} B_n(t) = \bigtriangledown^j B_{n-j}(t), \quad t \in \mathbb{R}. \tag{2.31}$$

The B-splines satisfy the recursive formula

$$B_n(t) = \frac{t}{n-1} B_{n-1}(t) + \frac{n-t}{n-1} B_{n-1}(t-1), \quad t \in \mathbb{R}. \tag{2.32}$$

Such a recursive formula makes B-splines very convenient to use in applications. We also know that the cardinal B-splines are symmetric about the center of their support; i.e.,

$$B_n\Big(\frac{n}{2} + t\Big) = B_n\Big(\frac{n}{2} - t\Big), \quad t \in \mathbb{R}. \tag{2.33}$$

We will see that these properties carry over to the Hilbert transform of B-splines. Using the recursive definition of the cardinal B-splines and the properties of the Hilbert transform, we have that

$$\mathcal{H}B_n(t) = \mathcal{H}B_{n-1} * B_1 = \mathcal{H}B_1 * B_{n-1}, \tag{2.34}$$

where $\mathcal{H}B_1$ has a specific expression given by

$$\mathcal{H}B_1(t) = \frac{1}{\pi} \ln \left| \frac{t}{t-1} \right| . \tag{2.35}$$

For the derivative of $\mathcal{H}B_1$, we obtain the formula

$$\frac{d}{dt}\mathcal{H}B_1(t) = \frac{1}{\pi t} - \frac{1}{\pi(t-1)}. \tag{2.36}$$

This formula can be generalized to the high order derivative of the Hilbert transform of B-splines of a higher order. In the following theorem, we show that the j-th derivative of the Hilbert transform of B_n is the j-th backward difference of $\mathcal{H}B_{n-j}$.

Theorem 2.1: *Let n be a positive integer. Then, the following statements hold.*

(i) *For any positive integer j with $j \le n$,*

$$\frac{d^j}{dt^j}\left(\mathcal{H}B_n\right)(t) = \nabla^j \mathcal{H}B_{n-j}(t). \tag{2.37}$$

(ii) *The Hilbert transform of cardinal B-splines have a recursive formula*

$$\mathcal{H}B_n(t) = \frac{t}{n-1}\mathcal{H}B_{n-1}(t) + \frac{n-t}{n-1}\mathcal{H}B_{n-1}(t-1), \quad t \in \mathbb{R}. \tag{2.38}$$

(iii) *The Hilbert transform of the cardinal B-splines B_n is anti-symmetric about the middle point $n/2$ of the support of B_n; that is*

$$\mathcal{H}B_n\Big(\frac{n}{2}+t\Big) = -\mathcal{H}B_n\Big(\frac{n}{2}-t\Big), \quad t \in \mathbb{R}. \tag{2.39}$$

We remark that it follows from part (iii) of the last theorem that $\mathcal{H}B_n$ has a zero at $n/2$.

The analytic signal of the cardinal B-spline B_n is defined by

$$Z_n(t) := B_n(t) + i\mathcal{H}B_n(t), \quad t \in \mathbb{R}. \tag{2.40}$$

This definition immediately implies that

$$Z_1(t) = \chi_{[0,1]}(t) + \frac{i}{\pi}\ln\left|\frac{t}{t-1}\right|. \tag{2.41}$$

The properties of B-splines and the Hilbert transform of B-splines are translated to Z_n, which we present in the following theorem.

Theorem 2.2: *The following statements hold for the analytic signal Z_n of the cardinal B-spline B_n:*

(i) *The function Z_n has the convolution property*

$$Z_n = B_1 * Z_{n-1} = Z_1 * B_{n-1}; \tag{2.42}$$

(ii) *The derivative of Z_n satisfies the relation*

$$\frac{d^j}{dt^j}Z_n(t) = \nabla^j Z_{n-j}(t), \quad t \in \mathbb{R}; \tag{2.43}$$

(iii) *The function Z_n may be computed by using the recursive formula*

$$Z_n(t) = \frac{t}{n-1} Z_{n-1}(t) + \frac{n-t}{n-1} Z_{n-1}(t-1), \quad t \in \mathbb{R}. \tag{2.44}$$

In practice, the spline representation obtained from the EMD method has non-uniform knots. Hence, it is desirable to consider the Hilbert transform of B-splines with non-uniform knots. In this case, we have the recurrence relation of (2.7). It is also known that the derivative of a B-spline can be written as a combination of lower-order B-splines:

$$B'_{j,k,\tau}(t) = (k-1)\left[\frac{B_{j,k-1,\tau}(t)}{\tau_{k+j-1} - \tau_j} - \frac{B_{j+1,k-1,\tau}(t)}{\tau_{k+j} - \tau_{j+1}}\right]. \tag{2.45}$$

Chen et al. (2004) proved that the Hilbert transform of B-splines has exactly the same recursive relation as the B-splines.

Theorem 2.3: (i) *The Hilbert transforms of B-splines satisfy the recursion relations*

$$\mathcal{H}B_{j,k,\tau}(t) = \frac{t-\tau_j}{\tau_{j+k-1} - \tau_j} \mathcal{H}B_{j,k-1,\tau}(t) + \frac{\tau_{j+k} - t}{\tau_{j+k} - \tau_{j+1}} \mathcal{H}B_{j+1,k-1,\tau}(t) \tag{2.46}$$

with

$$\mathcal{H}B_{j,1,\tau}(t) = \frac{1}{\pi} \ln\left|\frac{t-\tau_j}{t-\tau_{j+1}}\right|. \tag{2.47}$$

(ii) *The derivative of the Hilbert transform of B-splines satisfies the formula*

$$\frac{d}{dt}(\mathcal{H}B_{j,k,\tau})(t) = (k-1)\left[\frac{\mathcal{H}B_{j,k-1,\tau}(t)}{\tau_{k+j-1} - \tau_j} - \frac{\mathcal{H}B_{j+1,k-1,\tau}(t)}{\tau_{k+j} - \tau_{j+1}}\right]. \tag{2.48}$$

This recursive formula can be used to compute the Hilbert transform of B-splines of a higher order from the Hilbert transform of B-splines of a lower order.

The Bedrosian type formula (cf., Bedrosian 1963) plays a crucial role in computing the Hilbert transform of a product of two functions. This formula presents that the Hilbert transform of the product of a signal with lower frequency and one with higher frequency is equal to the signal with lower frequency times the Hilbert transform of the one with higher frequency. In the rest of this section, we show the validity of the Bedrosian type formula (cf., Bedrosian 1963) of the product of a polynomial and a signal having vanishing moments. Our consideration of a product of this type is motivated by an important characteristic of IMFs. We have seen either numerically or theoretically that an IMF has vanishing moments of a certain order. Specifically, we proved in Chen et al. (2004) that if a function has vanishing moments of order k, then the Hilbert transform of the product of this function with a polynomial of degree k is equal to the product of the polynomial and the Hilbert transform of this function.

For this purpose, we define the vanishing moments in the sense of the Cauchy principal value. We say a function f has vanishing moments of order k in this sense if the principal value integrals satisfy

$$PV \int_{\mathbb{R}} t^j f(t)\, dt = 0, \qquad 0 \le j \le k-1\,. \tag{2.49}$$

It can be readily verified that the basic harmonic signal $\cos(\omega_0 t)$ has vanishing moments of order 2 if $\omega_0 \neq 0$. Because of this property, the Bedrosian formula holds for the Hilbert transform of this function. We state this result in the next proposition.

Proposition 2.4: *Let $\omega_0 \neq 0$ and p_2 be a polynomial of degree 2. Then, the Bedrosian type formula holds*

$$\mathcal{H}\left[p_2(\cdot)\cos(\omega_0 \cdot)\right](t) = p_2(t)\sin(\omega_0 t)\,. \tag{2.50}$$

Moreover, we have the stronger result that this property holds for a general function having vanishing moments of order k.

Theorem 2.5: *Let f be a real valued function having vanishing moments of order k in the principal value sense. Then, for any polynomial p_n with degree $n \le k$, there holds the Bedrosian type formula*

$$\mathcal{H}(p_n f) = p_n \mathcal{H} f\,. \tag{2.51}$$

Recently, Xu and Yan (2004) studied the necessary and sufficient conditions which ensure the validity of the Bedrosian identity of the Hilbert transform of product functions fg. These authors presented convenient sufficient conditions, which cover the classical Bedrosian theorem and provide new additional insightful information. We now review the results from Xu and Yan (2004).

Theorem 2.6: *Let $f \in W^{1,2}(\mathbb{R})$ and $g, fg, fH(g) \in L^2(\mathbb{R})$. Then the Hilbert transform of function fg satisfies the Bedrosian identity*

$$H(fg) = fH(g) \tag{2.52}$$

if and only if

$$\int_0^1 \int_{\mathbb{R}} \frac{\omega}{t^2} e^{-2i\pi x\omega(t-1)/t} \hat{f}\left(\frac{\omega}{t}\right) \overline{\hat{g}(\omega)}\, d\omega\, dt = 0\,. \tag{2.53}$$

For a nonempty set $\Omega \subseteq \mathbb{R}$ and a real number t, we let

$$t\Omega := \{tx : x \in \Omega\}\,, \tag{2.54}$$

and for the unit interval $I := [0,1]$, we define the product set $I \cdot \Omega$ by

$$I \cdot \Omega := \bigcup_{t \in [0,1]} t\Omega\,. \tag{2.55}$$

The following result is a direct consequence of Theorem 2.6.

Proposition 2.7: *Let $f \in W^{1,2}(\mathbb{R})$ and $g, fg, fH(g) \in L^2(\mathbb{R})$. If*

$$(I \cdot \operatorname{supp}(\hat{f})) \cap \operatorname{supp}(\hat{g}) = \emptyset\,, \tag{2.56}$$

then the Hilbert transform of function fg satisfies the Bedrosian identity (2.52).

The classical Bedrosian theorem follows immediately from Proposition 2.7.

Corollary 2.8: *Let $a > 0$ and suppose that $f, g \in L^2(\mathbb{R})$ with*

$$\operatorname{supp}(\hat{f}) \subseteq (-a, a) \quad \text{and} \quad \operatorname{supp}(\hat{g}) \subseteq (-\infty, -a) \cup (a, \infty)\,. \tag{2.57}$$

Then, the Hilbert transform of function fg satisfies the Bedrosian identity (2.52).

Xu and Yan (2004) proved the following lemma and used it to relax the hypothesis of Proposition 2.7 on the function f.

Lemma 2.9: *If $f \in L^2(\mathbb{R})$ satisfies the condition that*

$$(I \cdot \operatorname{supp}(f)) \cap K = \emptyset \tag{2.58}$$

for some closed set K, then for any $\varepsilon > 0$, there exists $\varphi \in \mathcal{D}(\mathbb{R})$, the space of functions of bounded supports in C^∞, such that

$$\|f - \varphi\|_2 < \varepsilon \tag{2.59}$$

and

$$(I \cdot \operatorname{supp}(\varphi)) \cap K = \emptyset\,. \tag{2.60}$$

Theorem 2.10: *Let $f \in L^2(\mathbb{R})$, $g \in L^2(\mathbb{R}) \cap L^\infty(\mathbb{R})$ and $H(g) \in L^\infty(\mathbb{R})$. If condition (2.56) holds, then the Hilbert transform of functions fg satisfies the Bedrosian identity (2.52) almost everywhere.*

2.4. Performance analysis of BS-EMD

The EMD method decomposes a signal based on its intrinsic time scales. The energy of the IMFs with different local scales is distributed in different frequency bands. Numerical analysis has shown that for white and colored stationary noise, the original EMD acts as a dyadic filter bank, similar to the dyadic wavelet transform (Wu and Huang 2004; Flandrin et al. 2003). Here we present our research results on the behavior of the BS-EMD in this aspect. Most of the results have been reported in Liu et al. (2004). Our numerical experiment was carried out as follows. First, we generated 3000 independent Gaussian white noise time series of length 1024. Each was decomposed by using BS-EMD. Corresponding to each mode of the decomposition, the IMF was windowed and Fourier transformed. Then, we estimated the

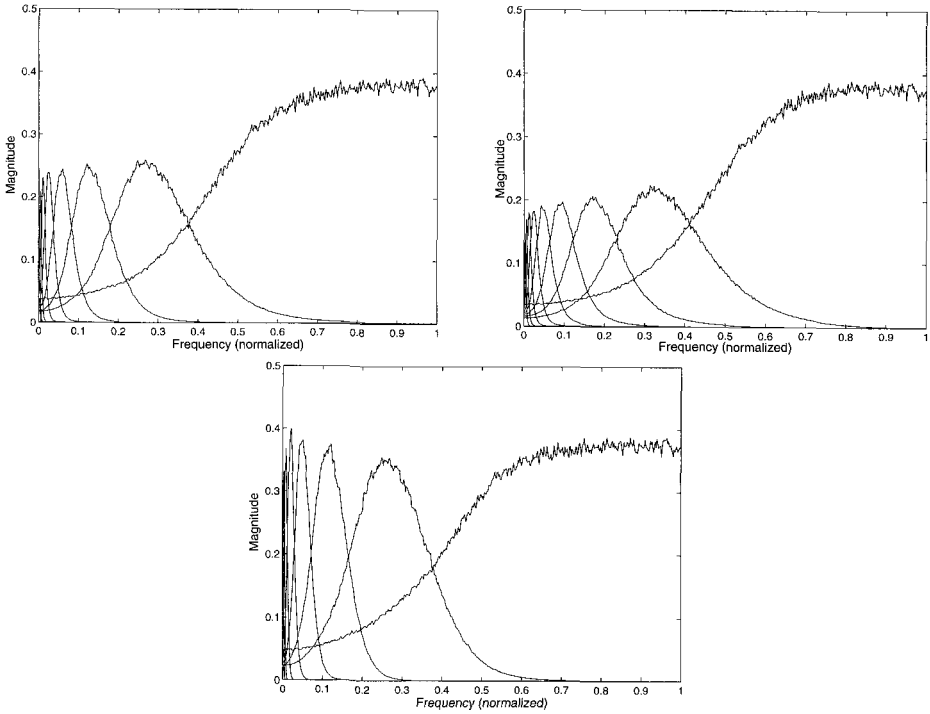

Figure 2.2: Power spectra of the IMFs obtained by using the cubic B-spline EMD (a, top left) the quadratic B-spline EMD (b, top right), and the original EMD (c, bottom). In each figure, from the right to the left, the first curve (half-bell shaped) is the power spectrum corresponding to IMF1, the second curve is that corresponding to IMF2, and so forth.

power spectrum for each mode as the average of the squared absolute values of the corresponding Fourier transforms over all the realizations.

Figures 2.2a–b show the estimated power spectra corresponding to the cubic and quadratic B-spline EMD respectively, where each curve corresponds to one decomposition mode. All the curves together in each figure can be interpreted as the frequency output of an equivalent filter bank. For comparison, Figure 2.2c presents the power spectra corresponding to the original EMD obtained by using the same procedure. One can see that the BS-EMD behaves similarly to the original EMD.

We now provide an interpretation of the properties of the BS-EMD as a filter bank. A rigorous mathematical proof requires further research. Consider a signal composed of a high frequency sinusoid riding on a low frequency sinusoid, as shown in Figure 2.3a, where the local extrema are marked by "o". From (2.10), we know that the coefficients of the B-splines in the operator defined by (2.11) are essentially the output of a low-pass filter applied to the local extremum sequence; the low-pass filter here is the binomial average. For the quadratic and cubic B-spline operators, the filters are $\{0.5, 0.5\}$ and $\{0.25, 0.5, 0.25\}$, respectively. In other words, the coefficient sequence in (2.11) is a smoothed version of the local extremum sequence

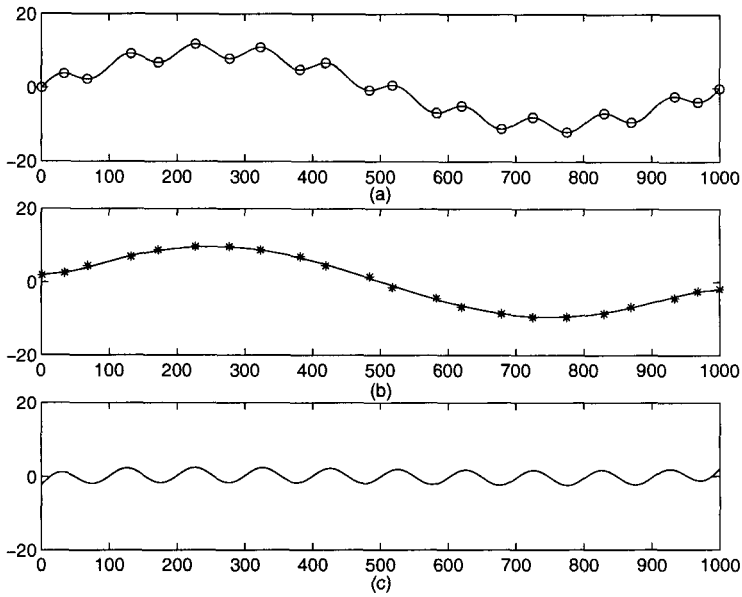

Figure 2.3: (a) Top. A signal composed of a high-frequency sinusoid riding on a low-frequency sinusoid, where the local extrema are marked by "o". (b) Middle. The waveform obtained by applying the operator defined in (2.11) to the signal. The points "*" represent the coefficients of the operator. (c) Bottom. The difference between the signal and the waveform in (b).

and represents the low frequency part of the latter. Furthermore, it has been proved that a function represented in the form of (2.11) does not have more sign changes than the coefficient sequence itself (De Boor 1978). We may thus consider that the component obtained by the operator of (2.11) represents the low-frequency part of the signal. Figure 2.3b shows such a component of the signal depicted in Fig. 2.3a obtained by using the cubic B-spline EMD, where the coefficients of the operator are represented by "*". The high frequency part of this signal obtained by subtraction of the low-frequency part is shown in Fig. 2.3c. In the next iteration, a new low-frequency part is generated from the current high-frequency part. When the stoppage criterion is satisfied, we obtain a high-frequency part, i.e., the first IMF, and the difference between the signal and the IMF, which is equal to the sum of the low-frequency parts generated in all the iterations. The next IMF is obtained in the same way except that it is extracted from the current low-frequency part. One can imagine that when all the IMFs are obtained, the signal will be decomposed into a number of frequency bands similar to those in a wavelet transform.

We should point out that like the original EMD, the BS-EMD decomposes a signal based on its local time scales. As such, the BS-EMD is a time-varying filter bank that is adaptive to the local time scales of a signal. This capability is different from that of a wavelet transform, in which the filter bank is predetermined. Consider a signal whose first half is a high-frequency sinusoid and second half, a low-frequency sinusoid. Differing from the frequencies and bandwidths of a wavelet transform, the

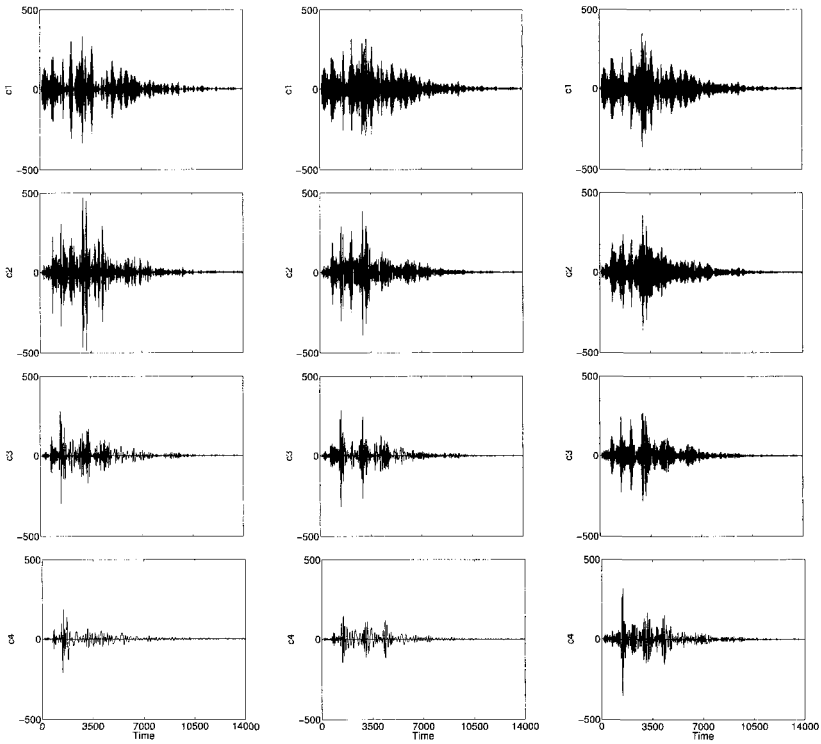

Figure 2.4: Plot of the first 4 IMFs for the earthquake data by the original EMD on the left, by the cubic B-spline EMD in the center, and by the quadratic B-spline EMD on the right.

central frequencies and bandwidths of the BS-EMD filter bank will change from the first to the second halves of the signal. For a white noise signal, the local scale varies randomly. The results presented in Figs. 2.2a–c thus are not applicable to a specific realization of the random process. They describe only the "average behavior" of the EMD as a filter bank.

We present another example, based on Chen et al. (2004), to further investigate the performance of the BS-EMD. The signal in the analysis is an earthquake record from the Chi-Chi event discussed originally by Huang et al. (2001). Our intention is not to decipher the meaning of the results, but merely to show that the BS-EMD can give similar results as the original EMD. In Figs. 2.4–2.6, the plots on the left are for the original envelope method, the plots in the center are for the cubic B-spline EMD, while the plots on the right are for the quadratic B-spline EMD. The residues are given separately in Fig. 2.7. As one can see, the original EMD produces only 10 IMF components, while the cubic and quadratic B-spline produce 11 and 12 IMF components, respectively. With averaging as in the B-spline, the wave groups tend to persist longer temporally and also through many different IMF components. As a result, the B-spline approaches would give a finer decomposition than the

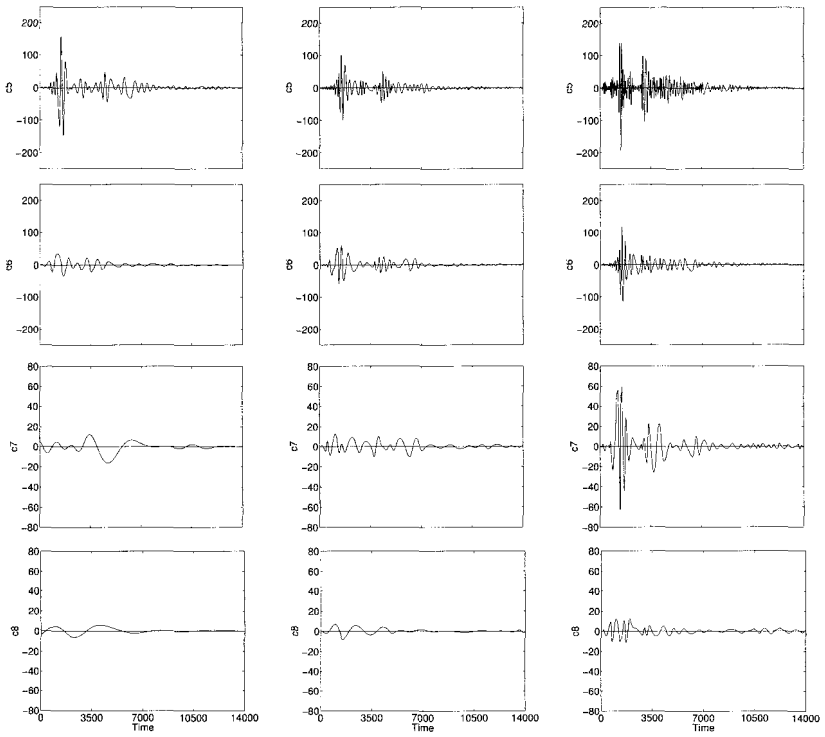

Figure 2.5: Plot of the next 4 IMFs for the earthquake data from the original EMD on the left, from the the cubic B-spline EMD in the center, and from quadratic B-spline EMD on the right.

envelope approach. However, the similarity between the envelope and the cubic B-spline approaches is evident. Even the last three components and the residues are qualitatively and quantitatively similar.

To evaluate the performance of the BS-EMD more accurately, we present the results of our investigation on the extent of the orthogonality among the IMFs and the energy conservation of the decompositions (Chen et al. 2004). The measures for orthogonality are defined by

$$IO_{max} := \max_{k \neq j} \frac{| < c_j, c_k > |}{\|c_j\|_2 \, \|c_k\|_2}, \qquad IO_{ave} = Average_{k<j} \frac{| < c_j, c_k > |}{\|c_j\|_2 \, \|c_k\|_2}. \tag{2.61}$$

We compute the sum of squared values of the IMFs and divide it by the squared values of the original signal minus the residue

$$IEC := \frac{\sum_t \sum_j |c_j(t)|^2}{\sum_t |s(t) - r(t)|^2} \tag{2.62}$$

to obtain an index of energy conservation. The latter reflects the fact that the sum of the IMFs represent the signal minus the trend given in the residue. For the earthquake signal, we have

Method	IO_{max}	IO_{ave}	IEC
Cubic spline	0.6111	0.0523	1.1439
Cubic B-spline	0.3334	0.0579	1.0459
Quadratic Bspline	0.3034	0.0519	1.2916

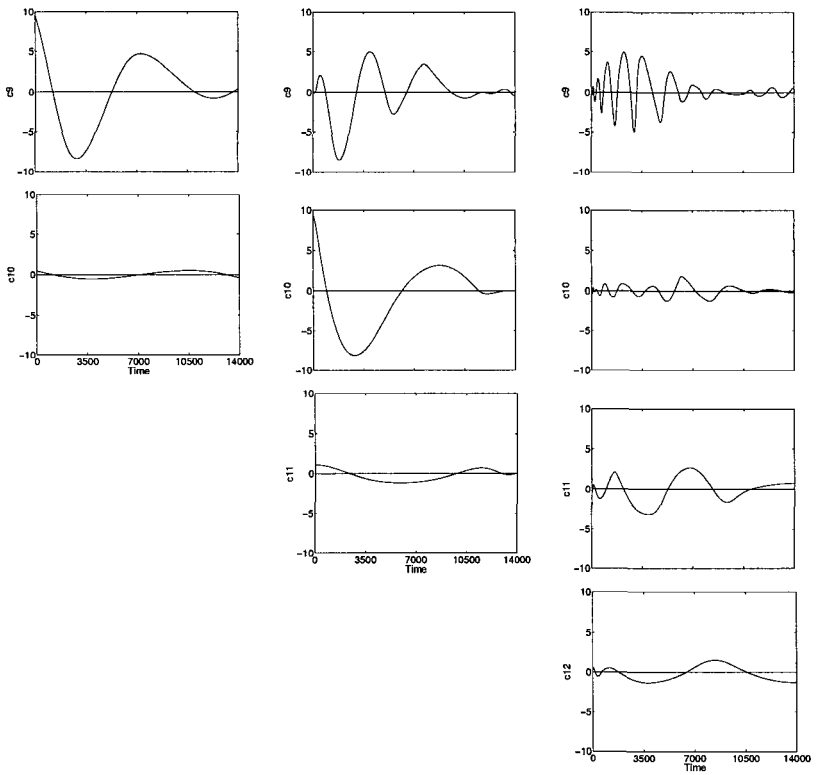

Figure 2.6: Plot of the last few IMFs for the earthquake data from the original EMD on the left, from the cubic B-spline EMD in the center, and from the quadratic B-spline EMD on the right.

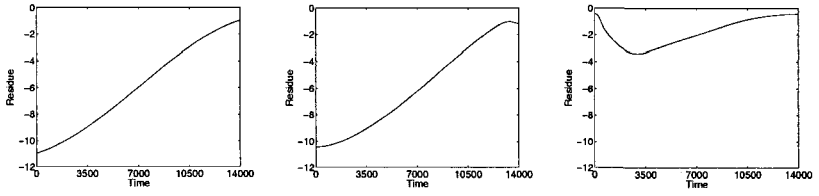

Figure 2.7: Plot of the residues for the earthquake data from the original EMD on the left, from the cubic B-spline EMD in the center, and from the quadratic B-spline EMD on the right.

The test results summarized in the above table show that the B-spline approaches give very comparable results to those of the original envelope approach. The cubic B-spline EMD performs especially well on the energy conservation test, and this finding indicates that the total energy deviation amongst the components is the smallest. The exact choice of the order of the B-spline is an open question. Although the lower order B-spline preserves local characteristics better, it will follow the data more closely. As our goal is to find the mean through the data, the higher order B-spline should give better mean and smaller orthogonal indices in both the maximum and average values. We thus recommend the cubic B-spline EMD as the choice for further mathematical investigation and applications.

2.5. Application examples

In this section, we present two application examples of the BS-EMD in transient detection. Transients are typical non-stationary signal components. The detection of such components is of interest in various applications. The problem investigated here is the detection of transients in vibration signals generated in mechanical systems. Our purpose is to diagnose incipient localized failures, which are a problem of great concern to industry (Braun 1986). When localized failures such as cracks and surface spalls exist in a mechanical system, the relatively-moving machine parts often impact one another. The impacts then excite transients into the background vibration. The detection of the transients is therefore a promising way to diagnose localized failures. However, doing so has been a challenging task because compared with the background vibration, the transients excited by incipient failures are usually very small. The results presented here show that the EMD techniques provide a promising tool for dealing with this problem.

The first example comes from Liu et al. (2004). The vibration signals in this example were collected from a fatigue test of an automobile gearbox. The transmission train had four pairs of gears. At the end of the test, one tooth of the driving gear in the last gear pair, which ran at 5.9 Hz, was broken. In the early stage of development, such a fault would excite a sequence of small transients into the background vibration. Our purpose is to detect the transients from the vibration signals collected before the breakage occurred. During this stage, a crack might be developing. In the test, the picked-up vibration signals were lowpass-filtered at 1.8 kHz and digitized at the sampling frequency of 4 kHz.

Figure 2.8a shows a signal collected before the tooth was broken. Since we are interested mainly in the time-frequency composition, the signal is normalized as unit energy for the sake of convenience. We also do so for the signal in the second application example presented later. The Fourier transform of the signal in Fig. 2.8a is given in Fig. 2.8b. It is difficult to understand the condition of the gearbox based directly on the Fourier transform. Figure 2.9 shows the first seven IMFs obtained by using the BS-EMD. One can see that IMFs 3–6 contain equally spaced impulses representing the transient components in the signal. It can be determined

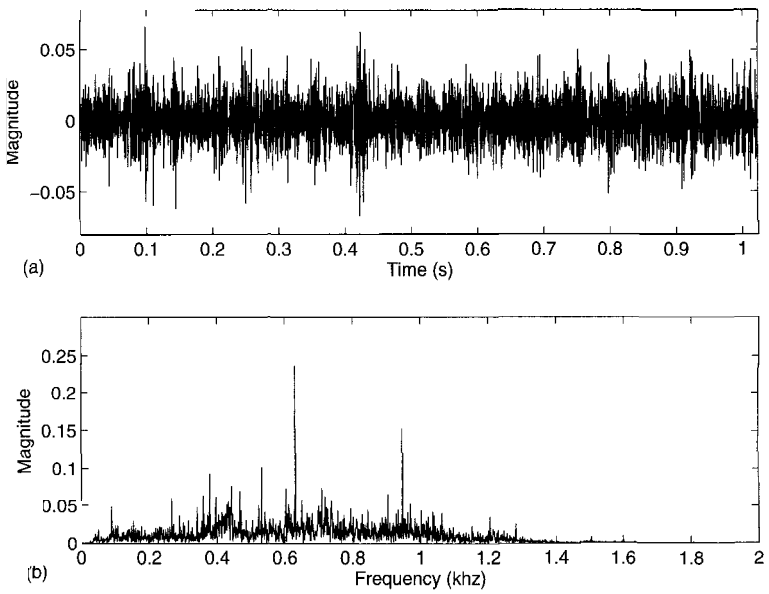

Figure 2.8: (a, top) A vibration signal collected from the gearbox with a tooth crack, and (b, bottom) its Fourier transform. The signal has been normalized as unit energy.

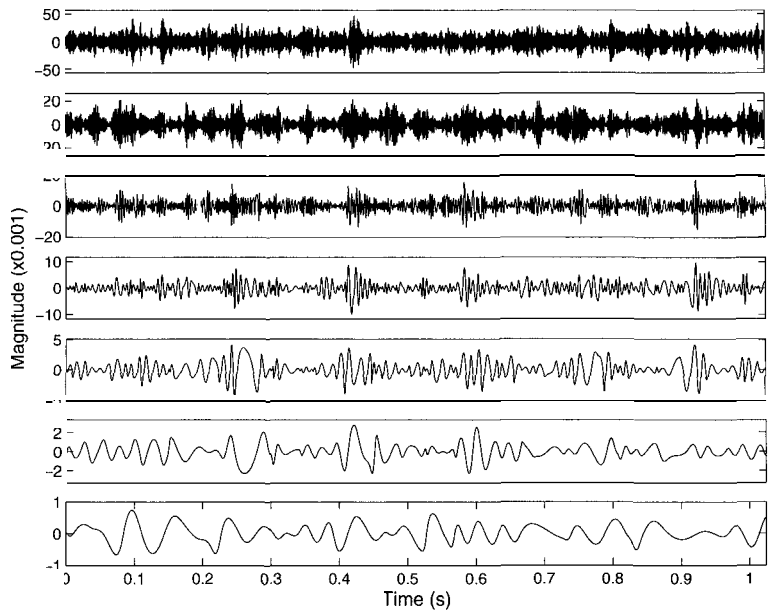

Figure 2.9: IMFs of the signal in Fig. 2.8a obtained by using the BS-EMD. The indexes of the IMFs increase from the top to the bottom.

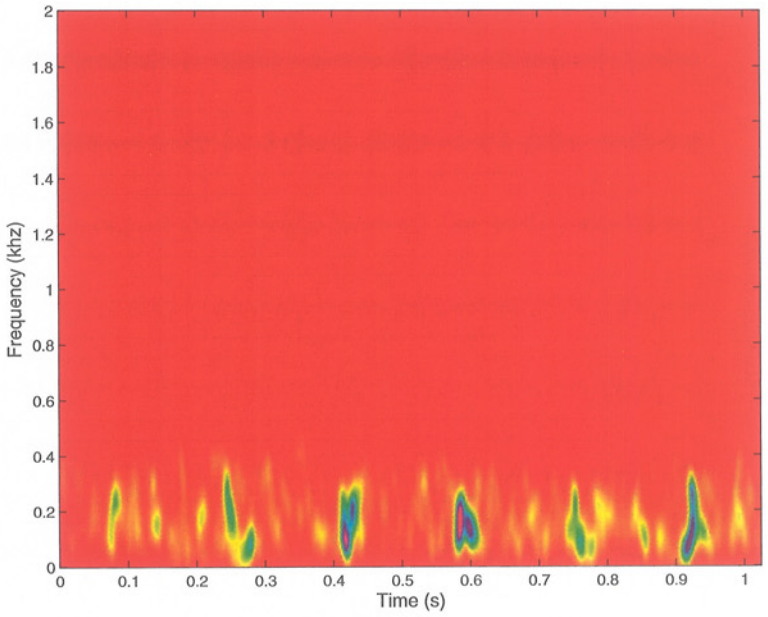

Figure 2.10: Hilbert spectrum of the third to sixth IMFs shown in Fig. 2.9.

that the transients are distributed over the frequency range of these four IMFs. The Hilbert spectrum obtained from the Hilbert transform of these four IMFs is given in Fig. 2.10, where the brighter patches show the time-frequency characteristics of the transients. For better identification of the featured components, a smoothed representation of the Hilbert spectrum is used in this section (see Huang et al. 1998). From Figs. 2.9 and 2.10, we can obtain the following information. Firstly, the average time spacing between the neighboring transients is about 0.17 s, corresponding to 5.9 Hz in frequency – the rotation frequency of the damaged gear. Secondly, the frequency of the impulses ranges from 0 to about 300 Hz and covers the sidebands of the meshing frequency of the last gear pair in the transmission path. This mesh frequency is about 88.4 Hz. Finally, the fifth IMF shows that a phase delay occurs in some of the impulses. Based on the general knowledge of gearbox diagnosis (Braun 1986), we know that these features indicate the existence of a localized defect on the driving gear of the last gear pair.

Figures 2.11 and 2.12 show the first seven IMFs and the Hilbert spectrum of IMFs 3–6 obtained by using the original EMD. For this specific signal, the IMFs and Hilbert spectrum obtained by using the BS-EMD appear to reveal the impulses better than those obtained by using the original EMD.

The problem that the second example involves is the localized failure diagnosis of a rolling element bearing through transient detection. The specifications of the bearing in the test were as follows: number of rolling elements, 8; diameter of the rolling elements, 15 mm; medium diameter, 65 mm; and contact angle, 0°. The bearing

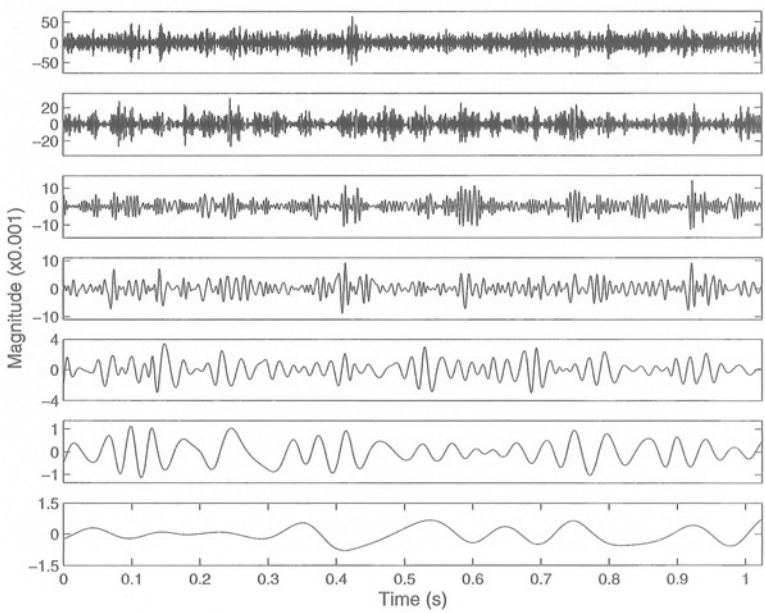

Figure 2.11: IMFs of the signal in Fig. 2.8a obtained using the original EMD. The indexes of the IMFs increase from the top to the bottom.

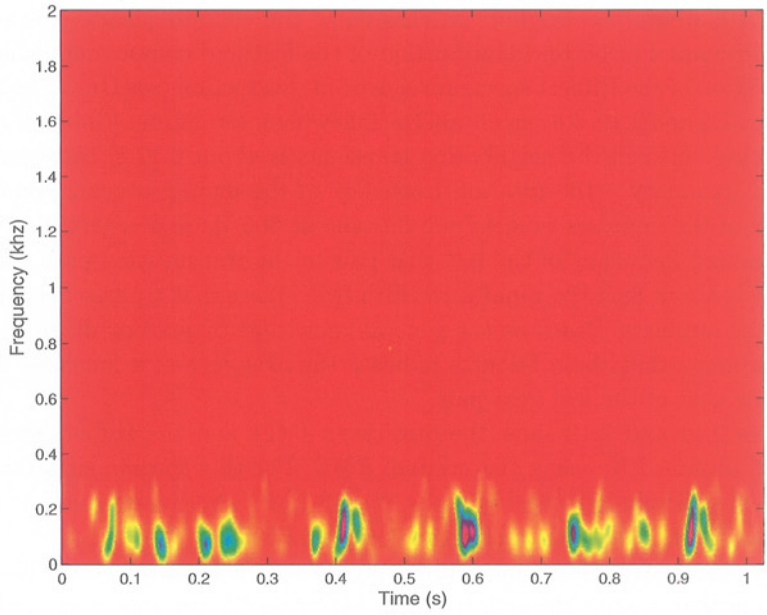

Figure 2.12: Hilbert spectrum of the third to sixth IMFs shown in Fig. 2.11.

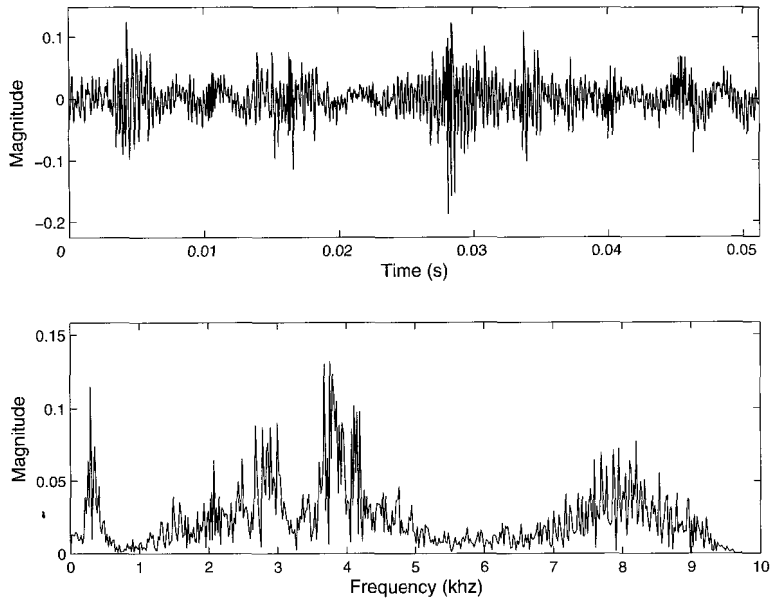

Figure 2.13: (a, top) A vibration signal collected from the bearing, and (b, bottom) its Fourier transform. The signal has been normalized as unit energy.

carried a defect on its inner race induced in the form of a dimple measuring about 0.1 mm in depth and 1 mm in diameter to simulate an incipient surface spalling. The vibration signals were picked up at a constant inner race rotation speed of 1900 rpm. They were lowpass-filtered at 9 kHz and digitized at the sampling rate of 20 kHz. An inner race defect could generate a sequence of high-frequency vibration transients. These transients are equally spaced in time but usually have different amplitudes and frequency ranges if the inner race rotates. Under the present test conditions, it can be computed that the average time spacing between the neighboring transients is 6.4 ms (Braun 1986).

Figure 2.13 shows a typical vibration record from the bearing and its Fourier transform. The signal contains some impulses and high-frequency components. These features more or less show the presence of a localized defect in the bearing. The IMFs obtained by using the BS-EMD are presented in Fig. 2.14, of which the first three IMFs better reveal the existence of the transients than the waveform of the original signal. Figure 2.15 shows the corresponding Hilbert spectrum. It reveals the corresponding frequency range of each transient. Some transients that are difficult to identify from the waveforms of the IMFs become clearer in the Hilbert spectrum, such as the transient represented by the bright patch close to the time instant of 0.01 s and in the frequency band from 7 kHz to 9 kHz. Figures 2.14 and 2.15 also reveal that the average time spacing between the neighboring transients is about 6 ms or its multiple. This value is close to the computed one mentioned above. Based on these features, the finding that the bearing carried a localized inner race defect is convincing.

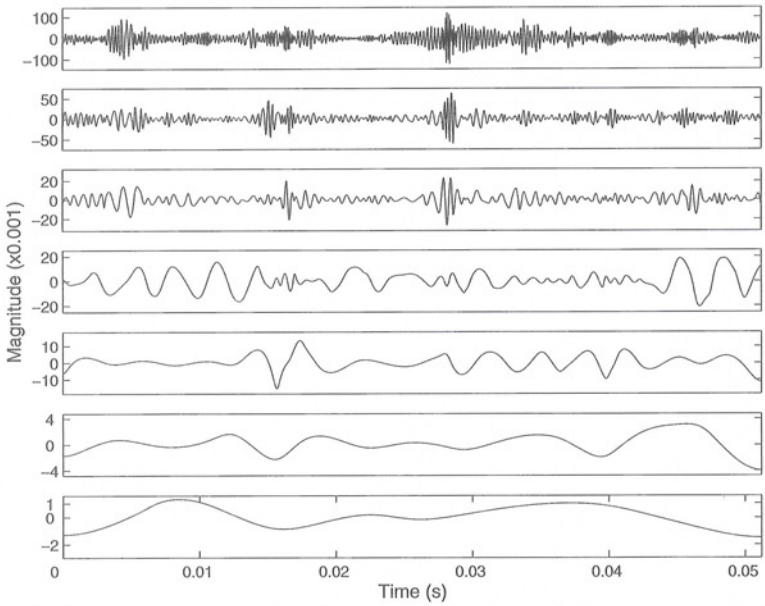

Figure 2.14: IMFs of the signal in Fig. 2. 13a obtained by using the BS-EMD. The indexes of the IMFs increase from the top to the bottom.

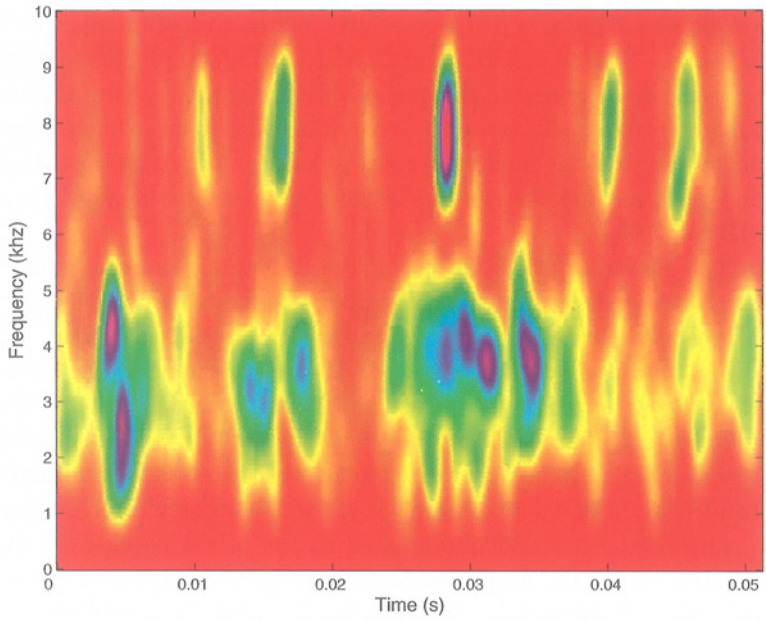

Figure 2.15: Hilbert spectrum of the first to third IMFs shown in Fig. 2.14.

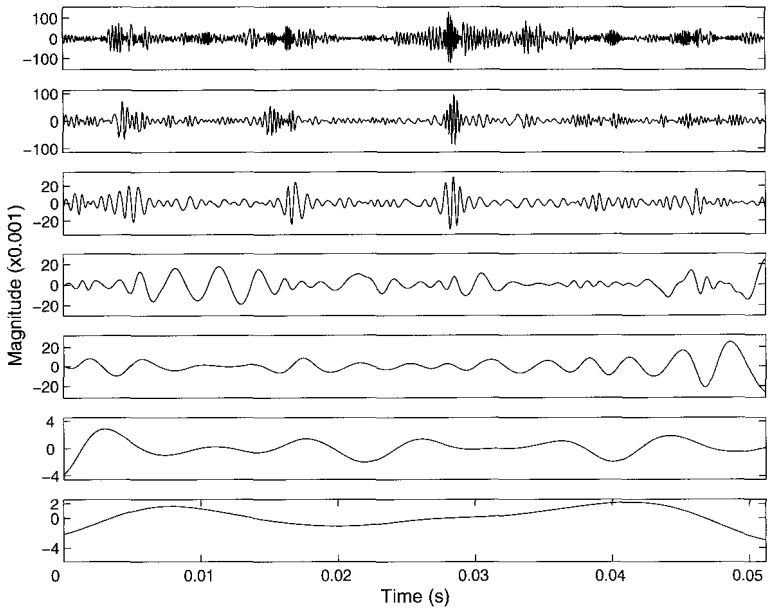

Figure 2.16: IMFs of the signal in Fig. 2.13a obtained using the original EMD. The indexes of the IMFs increase from the top to the bottom.

Figures 2.16 and 2.17 show the IMFs obtained by using the original EMD and the Hilbert spectrum computed from the first three IMFs. They provide similar information to that in Figs. 2.14 and 2.15. We have analyzed more signals. The results show that the performances of the two methods are generally comparable.

2.6. Conclusion and future research topics

The empirical mode decomposition and Hilbert spectral analysis, comprising the Hilbert–Huang transform, has been applied with great success for nonlinear and non-stationary signal analysis in various areas. However, most of the underlying mathematical problems have been left untreated. Given the rapid progress made in the methodology and applications, we urgently need to develop a firm mathematical foundation for the Hilbert–Huang transform. This paper reviewed the work in that direction based on Chen et al. (2004), Liu et al. (2004), and Xu and Yan (2004). We described the algorithm of our B-spline based EMD and presented the results of some related mathematical studies. The simulated and practical application examples given in the paper showed that the BS-EMD has a comparable performance to that of the original EMD. To facilitate future progress, we have identified the outstanding mathematical problems in Chen et al. (2004). We now summarize those problems closely related to the B-spline EMD.

In time-frequency analysis, traditional methods are often conducted with an *a priori* basis constructed based on certain general criteria. For nonlinear and non-stationary signals, which have varying local characteristics, it is impossible to expect

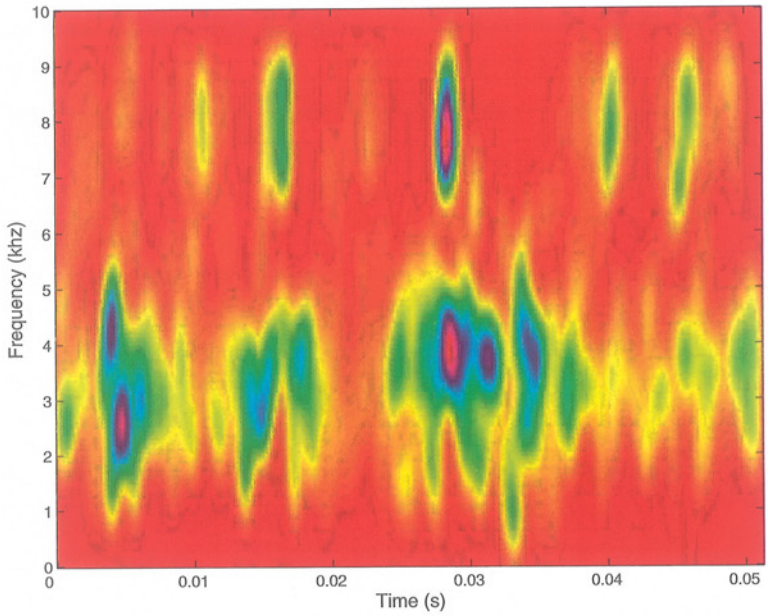

Figure 2.17: Hilbert spectrum of the third to sixth IMFs shown in Fig. 2.16.

a fixed basis to fit all the signals without invoking spurious harmonics. A breakthrough in improving the technology is the development of the adaptive representation methods using an over-complete basis library, e.g., Coifman et al. (1992), Mallat and Zhang (1993), Chen and Donoho (1995). They select from the library a basis that is "adapted" to the analyzed signal. These methods have good mathematical grounds but are not fully adaptive, for the library itself is *a priori*, and increasing the size of the library will result in computational difficulties. In the case of the EMD approach, the representation is general and adaptive enough but not mathematically rigorous. A fundamental reason for the latter is that the intrinsic mode functions lack a mathematically rigorous definition. This problem may be addressed within the B-spline EMD method, as all the intrinsic mode functions, other than the first one, obtained from either the original or the B-spline EMD can be represented as sums of B-spline curves.

For the same reason mentioned above, the B-spline EMD could also be used to address the problem of the convergence of EMD. By "convergence," we mean that the EMD will produce only a finite set of IMF components. Although all intuitive reasoning and numerical experiments suggest that the EMD procedure should be convergent, a general and complete proof is still wanting. In general, the cubic spline mean envelope could create extra extrema by itself. This possibility introduces more difficulties for attempts to prove the convergence. An expected benefit from using B-splines is that the convergence might come as a result of the nice variation-diminishing properties of B-spline series. Certainly, there still exist challenges, such as how to deal with the hidden scales caused by the inflection points in the data.

Several implementation issues need to be settled for the B-spline approach, just as they do for the envelope approach. Firstly, the B-spline EMD also depends on the stoppage criterion. Since different stoppage criteria yield different sets of IMFs, an optimal one is naturally desired. Secondly, although we have an intuitive reason, as mentioned in section 2.4, to choose a cubic B-spline for the BS-EMD, the exact choice of the order still remains a question. Finally, since we are dealing with finite data, our algorithm must also be adjusted to use some form of boundary conditions. Although one can invoke the "clamped" end point option to fix the ends, how to select the fixed end is still a problem. Even if the local modification property of the B-spline will limit the influence to the end regions, the region of influence will become larger and larger as the scale of the IMF mode becomes larger, and the influence of the ends will propagate into the low-frequency data components. Clearly, if the B-spline approach is to become a viable alternative to the envelope approach, a detailed investigation of these problems is urgently needed.

Although the B-spline approach has the same problems as the original approach concerning the above-mentioned issues, with the analytical form, the B-spline approach, however, is more amenable to mathematical analysis. The variation-diminishing properties and the partition of unity properties of the B-spline series may be particularly useful. With these advantages, the B-spline approach really deserves more detailed investigation.

Acknowledgements

This work was supported in part by National Aeronautics and Space Administration under grant NAG5-5364, and National Science Foundation under grants NSF0314742 and NSF0312113.

References

Bedrosian, E., 1963: A product theorem for Hilbert transform. *Proc. IEEE*, **51**, 868–869.

Braun, S., 1986: *Mechanical Signature Analysis.* Academic Press, 385 pp.

Chen, S., D. Donoho, and M. Saunders, 2001: Atomic decomposition by basis pursuit. *SIAM Rev.*, **43**, 129–159.

Chen, Q., N. E. Huang, S. Riemenschneider, and Y. Xu, 2004: A B-spline approach for empirical mode decompositions. *Adv. Comput. Math.*, in press.

Choi, H. I., and W. J. Williams, 1989: Improved time-frequency representation of multicomponent signals using exponential kernels. *IEEE Trans. Acoust. Speech Signal Process.*, **37**, 862–871.

Cohen, L., 1966: Generalized phase-space distribution functions. *J. Math. Phys. (Woodside, NY)*, **7**, 781–786.

Cohen, L., 1995: *Time-Frequency Analysis.* Prentice Hall, 299 pp.

Coifman, R. R., Y. Meyer, and M. V. Wickerhauser, 1992: Wavelet analysis and signal processing. *Wavelets and Their Applications*, M. B. Ruskai et al., Eds., Jones and Bartlett, 153–178.

Daubechies, I., 1992: *Ten Lectures on Wavelets*. CBMS-NSF Series in Applied Mathematics. Vol. 61, SIAM, 357 pp.

De Boor, C., 1978: *A Practical Guide to Splines*. Springer-Verlag, 392 pp.

Diks, C., 1999: *Nonlinear Time Series Analysis*. World Scientific Press, 220 pp.

Echeverria, J. C., J. A. Crowe, M. S. Woolfson, and B. R. Hayes-Gill, 2001: Application of empirical mode decomposition to heart rate variability analysis. *Med. Biol. Eng. Comput.*, **39**, 471–479.

Flandrin, P., G. Rilling, and P. Gonçalvès, 2004: Empirical mode decomposition as a filter bank. *IEEE Signal Process. Lett.*, **11**, 112–114.

Gabor, D., 1946: Theory of communications. *J. IEE*, **93**, 429–457.

Golitschek, M. V., 1972: On the convergence of interpolating periodic spline functions of high degree. *Numer. Math.*, **19**, 146–154.

Huang, N. E., Z. Shen, S. R. Long, M. C. Wu, H. H. Shih, Q. Zheng, N.-C. Yen, C. C. Tung, and H. H. Liu, 1998: The empirical mode decomposition and the Hilbert spectrum for nonlinear and non-stationary time series analysis. *Proc. R. Soc. London, Ser. A*, **454**, 903–995.

Huang, N. E., Z. Shen, and S. R. Long, 1999: A new view of nonlinear water waves: The Hilbert spectrum. *Annu. Rev. Fluid Mech.*, **31**, 417–457.

Huang, N. E., C. C. Chern, K. Huang, L. W. Salvino, S. R. Long, and K. L. Fan, 2001: A new spectral representation of earthquake data: Hilbert spectral analysis of Station TCU129, Chi-Chi, Taiwan, 21 September 1999. *Bull. Seism. Soc. Am.*, **91**, 1310–1338.

Jones, D. L., and T. W. Parks, 1990: A high resolution data-adaptive time-frequency representation. *IEEE Trans. Acoust. Speech Signal Process.*, **38**, 2127–2135.

Liu, B., S. Riemenschneider, and Y. Xu, 2004: Gearbox fault diagnosis using empirical mode decomposition and Hilbert spectrum. *Mech. Syst. Signal Process.*, in press.

Mallat, S., 1998: *A Wavelet Tour of Signal Processing*. Academic Press, 637 pp.

Mallat, S., and Z. Zhang, 1993: Matching pursuit with time-frequency dictionaries. *IEEE Trans. Signal Process.*, **41**, 3397–3415.

Pines, D., and L. Salvino, 2002: Health monitoring of one dimensional structures using empirical mode decomposition and the Hilbert–Huang transform. *Proc. SPIE*, **4701**, 127–143.

Qian, S., and D. Chen, 1996: *Joint Time-Frequency Analysis: Methods and Applications*. Prentice Hall, 302 pp.

Schoenberg, I. J., 1964: On interpolation by spline functions and its minimal properties. *On Approximation Theory (Proc. Oberwolfach Conf. 4–10 Aug. 1963)*, ISNM Vol. 5, Birkhäuser, 109–129.

Schoenberg, I. J., 1972: Notes on spline functions I: The limits of the interpolating periodic spline functions as their degree tends to infinity. *Indag. Math.*, **34**, 412–422.

Schoenberg, I. J., 1976: On the remainders and the convergence of cardinal spline

interpolation for almost periodic functions. *Studies in Spline Functions and Approximation*, S. Karlin et al., Eds., Academic Press, 277–303.

Schoenberg, I. J., 1983: A new approach to Euler splines. *J. Approx. Theory*, **39**, 324–337.

Ville, J., 1948: Théorie et applications de la notion de signal analytique. *Câbles Transmissions*, **2A**, 61–74.

Wigner, E. P., 1932: On the quantum correction for thermodynamic equilibrium. *Phys. Rev.*, **40**, 749–759.

Wu, Z., and N. E. Huang, 2004: A study of the characteristics of white noise using the empirical mode decomposition method. *Proc. R. Soc. London, Ser. A*, **460**, 1597–1611.

Xu, Y., and D. Yan, 2004: The Hilbert transform of product functions and the Bedrosian identity. Preprint, Department of Mathematics, Syracuse University, USA, 11 pp.

Zhang, R. R., S. Ma, and S. Hartzell, 2003: Signatures of the seismic source in EMD-based characterization of the 1994 Northridge, California, earthquake recordings. *Bull. Seism. Soc. Amer.*, **93**, 501–518.

Zhao, Y., L. E. Atlas, and R. J. Marks, 1990: The use of cone-shaped kernels for generalized time-frequency representations of non-stationary signals. *IEEE Trans. Acoust. Speech Signal Process.*, **38**, 1084–1091.

Sherman Riemenschneider
Department of Mathematics, West Virginia University, Morgantown, WV 26506, USA
sherm@math.wvu.edu

Bao Liu
Department of Mathematics, West Virginia University, Morgantown, WV 26506, USA
bliu@math.wvu.edu

Yuesheng Xu
Department of Mathematics, Syracuse University, Syracuse, NY 13244, USA
yxu06@syr.edu

Norden E. Huang
Goddard Institute for Data Analysis, Code 614.2, NASA/Goddard Space Flight Center Greenbelt, MD 20771, USA
norden.e.huang@nasa.gov